Sensors & Diagnostics



COMMUNICATION

View Article Online



Cite this: Sens. Diagn., 2025, 4, 574

Received 18th February 2025, Accepted 12th April 2025

A novel two-photon fluorescent probe for nondestructive imaging of Hg²⁺ in fresh plant tissues†

Xiao Liu,‡^a Zheng Zhu,‡^b Ruitao Sun,^a Jun Li*^a and Shengzhen Xu ¹⁰*

DOI: 10.1039/d5sd00023h

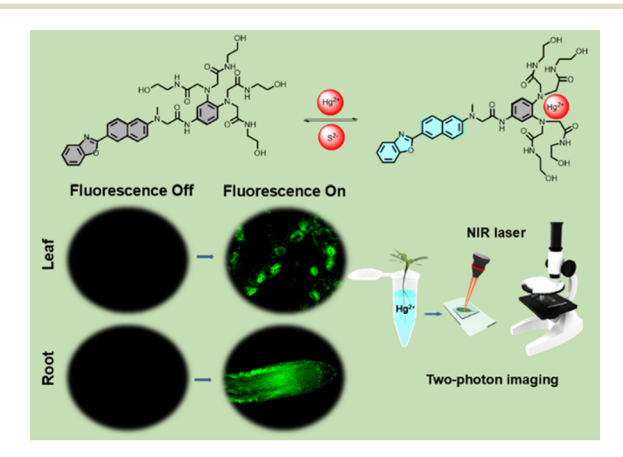
rsc li/sensors

In this work, we developed a small-molecule fluorescent probe (termed as LJTP3) for the specific detection of Hg2+ with high sensitivity in living plant tissues. LJTP3 can not only effectively indicate the spatiotemporal distribution of Hg2+ in the plant subcellular level, but also enable to realize 3D imaging of Hg²⁺ in plant roots.

Mercury, a highly toxic heavy metal, is widely distributed in the natural environment. However, with the increasing intensity of human activities such as industrial production, coal combustion, waste incineration and agricultural practices, mercury emissions have risen significantly, leading to serious environmental contamination. 1,2 As a major form of Hg, Hg²⁺ exhibited a strong affinity for proteins with bioaccumulation properties.3 As a critical component of ecosystems, plants are particularly sensitive to mercury pollution.4 Studies have shown that Hg2+ tends to accumulate in plant roots and leaves, and elevated levels can cause visible damage to plant tissues and further affect plant growth and crop production.5,6 Therefore, developing an efficient tool for the detection of Hg^{2^+} in plants has great significance for agricultural management.

During the past decades, various traditional methods for detecting Hg²⁺ have been developed, including but not limited to inductively coupled plasma atomic emission spectrometry (ICP-AES), inductively coupled plasma mass spectrometry (ICP-MS), atomic fluorescence spectrometry (AFS), atomic absorption spectrometry (AAS), and chemiluminescence methods.^{7–10} Compared to these fluorescence displayed distinct sensors advantages, such as high sensitivity, superior spatiotemporal

In this study, a water-soluble fluorescent probe, LJTP3 was tailored for the detection and imaging of Hg2+ in plant tissues. It comprises a 2-(naphthalen-2-yl)benzo[d]oxazolebased fluorophore for signal output, and a hydrophilic tetrakis(N-2-hydroxyethyl)acetamide group as the Hg2+ specific binding component. LJTP3 exhibited not only excellent selectivity but also a low detection limit (LOD) of 0.08 µM for the early detection of Hg²⁺. Moreover, the



Scheme 1 Illustration of a two-photon fluorescent probe (LJTP3) for the detection of Hg²⁺ in Arabidopsis thaliana.

resolution, and non-invasive in situ imaging capabilities. 11-15 As a result, several fluorescent probes have been employed for the in vivo detection of Hg²⁺. 16-21 However, only a few small-molecule organic fluorescent probes have been reported to achieve clear imaging at subcellular levels in plants. 22-28 In particular, two-photon fluorescent probes possess NIR excitation wavelengths, enabling deeper penetration into plant tissues to achieve plant subcellular imaging with minimum interference of background. However, two-photon-based small-molecule probes for subcellular imaging in plants are still few, and the dynamic distribution of Hg2+ at subcellular lever still needs to be further investigated.29-32

^a College of Chemistry, Huazhong Agricultural University, Wuhan, Hubei 430070, China. E-mail: xusz@mail.hzau.edu.cn

^b College of Life Science and Technology, Huazhong Agricultural University, Wuhan, Hubei 430070, China

[†] Electronic supplementary information (ESI) available. See DOI: https://doi.org/ 10.1039/d5sd00023h

[‡] X. Liu and Z. Zhu contributed equally to this work.

fluorescence signals for Hg2+ detection were observed in the model plant Arabidopsis, allowing visualization of its localization at the subcellular level. More importantly, the temporal and spatiotemporal distribution of mercury (Hg) was clearly observed under two-photon microscopy and 3D reconstruction (Scheme 1).

The synthetic procedures of LJTP3 are shown in Scheme S1 (ESI†) and the molecular characterization data are shown in Fig. S1-S17 (ESI†). The synthesis of LJTP3 was ultimately achieved through an 8-step process involving nucleophilic substitution, nitration, reduction, and condensation reactions to get the probe with moderate yields.

Following the successful synthesis of LJTP3, evaluation of its response to Hg²⁺ was then performed in HEPES solution. As shown in Fig. S18 (ESI†), the probe itself has an obvious UV absorption peak at 355 nm in HEPES solution, which was employed as the excitation wavelength of LJTP3. The fluorescence titration experiment of LJTP3 revealed that only Hg²⁺ induced significant fluorescence enhancement at the emission peak of 480 nm, while other metal ions including Ag⁺, Ba²⁺, Ca²⁺, Cr³⁺, Cd²⁺, Fe²⁺, Fe³⁺, Mg²⁺, Mn²⁺, Na⁺, Pd²⁺, and Zn²⁺ did not induce obvious fluorescence enhancement, indicating the good selectivity of LJTP3 (Fig. 1A). In addition, fluorescence interference tests for different ions were carried out in HEPES solution. As shown in Fig. 1B, the fluorescence of the probe LJTP3 shows minimal interference from other coexisting metal ions, demonstrating its strong anti-interference capability. This suggests that LJTP3 can be well-suited for the selective

detection of Hg2+ in complex systems. The fluorescence spectra of the probe LJTP3 (1 µM) were measured at varying concentrations of Hg^{2+} (0-10 μ M), as shown in Fig. 1C. The fluorescence intensity gradually increased with increasing Hg2+ concentrations, until reaching a plateau. During the titration experiments, a good linear relationship was observed between the fluorescence intensity concentrations of Hg^{2+} in the range of 0-3 μM (Fig. 1D). The limit of detection (LOD) was determined to be 0.08 µM.

The binding mode of the probe LJTP3 for Hg2+ was hypothesized, as shown in the Fig. S19.† Upon coordination of the polyamide ligands with Hg2+, the PET effect was weakened, leading to enhance fluorescence intensity. To confirm this hypothesis, the detection mechanism of LJTP3 toward Hg²⁺ was thoroughly validated using ESI-MS. As shown in Fig. S20 (ESI \dagger), the molecular ion peak (m/z: 1044.3536) was observed, which matches the calculated value (m/z: 1044.3538).

Additionally, a Job-plot experiment was conducted (Fig. 1F). The intersection of the curve at a ratio of 0.5 indicates a 1:1 binding ratio between LITP3 and Hg²⁺. Due to its specific affinity for S²⁻, the Hg²⁺-enhanced fluorescence was restored to the level of the free probe. This rapid and reversible sensing behavior was repeated five times without significant signal attenuation (Fig. 1E), confirming the reversibility of the binding. Besides, LJTP3 exhibited high stability within the pH range of 6.5-8.0, making it suitable for Hg²⁺ sensing under physiological conditions (Fig. S21 ESI†).

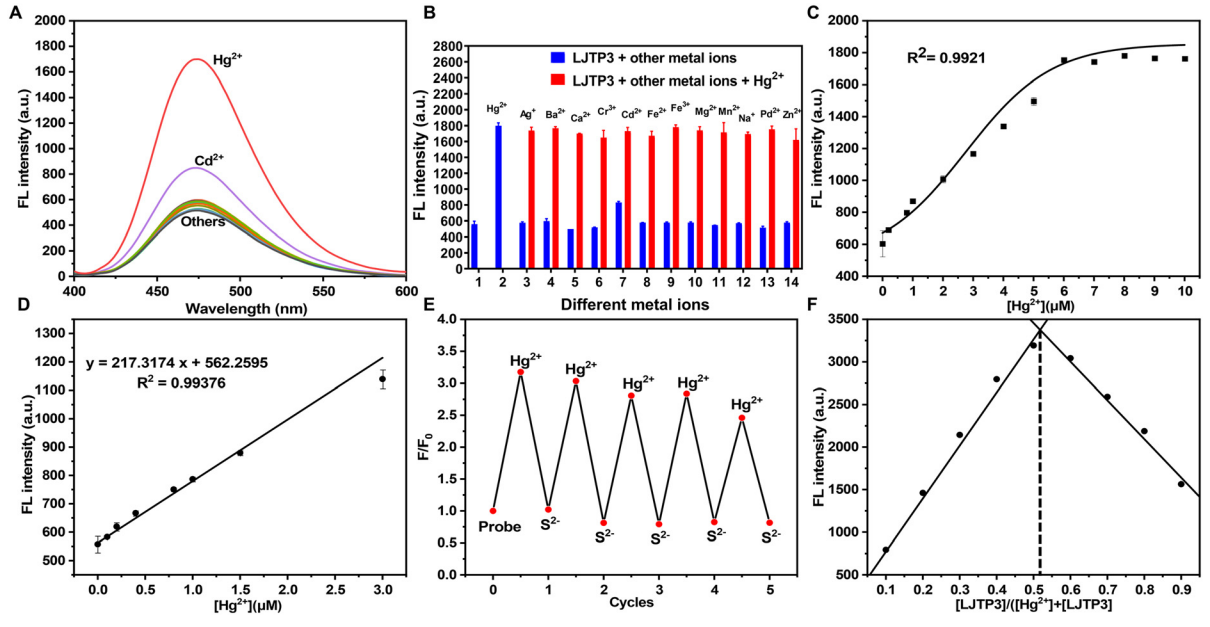
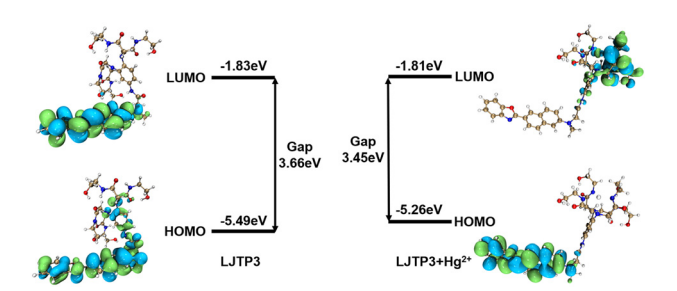


Fig. 1 (A) Fluorescence response of LJTP3 (1 μ M) towards various metal ions (10 μ M), including Hg²⁺, Ag⁺, Ba²⁺, Ca²⁺, Cr³⁺, Cd²⁺, Fe²⁺, Fe³⁺, Mg²⁺, Mn²⁺, Na⁺, Pd²⁺, and Zn²⁺. (B) Fluorescence selectivity of LJTP3 (1 μM) with Hg²⁺ (10 μM) in the presence of various metal ions (10 μM), including 1. the probe only, 2. Hg²⁺, 3. Ag⁺, 4. Ba²⁺, 5. Ca²⁺, 6. Cr³⁺, 7. Cd²⁺, 8. Fe²⁺, 9. Fe³⁺, 10. Mg²⁺, 11. Mn²⁺, 12. Na⁺, 13. Pd²⁺, and 14. Zn²⁺. (C) Fluorescence titration of LJTP3 (1 μ M) with different concentrations of Hq²⁺. (D) Linear relationship of LJTP3 with different concentrations of Hq²⁺ in the range of 0-3.0 μ M. (E) Fluorescence response of LJTP3 based on emission at 480 nm in cycles of Hg²⁺ (1 μ M) addition and subsequent Na₂S (1 μ M) treatment. (F) Job-plots of the fluorescence intensity of LJTP3.



Communication

Fig. 2 Molecular orbitals and corresponding energy levels of LJTP3 and LJTP3 + Hg²⁺ in both the ground state and excitation state.

To investigate the sensing mechanism (Fig. 2), density functional theory (DFT) calculations were performed using Gaussian 16 software.³³ The highest occupied molecular orbital (HOMO) and lowest unoccupied molecular orbital (LUMO) of LJTP3 were primarily localized on the fluorophore, although the HOMO also exhibited partial distribution in the recognition group. The energy gap between the HOMO and LUMO was calculated to be 3.66 eV, with photo-induced electron transfer (PET) occurring from the recognition group to the fluorophore, resulting in fluorescence quenching. Upon binding with Hg²⁺, the distribution of both the HOMO and LUMO shifted towards the fluorophore and recognition group, respectively, with a reduced energy gap of 3.45 eV, leading to the inhibition of PET and consequently, fluorescence restoration.

Given the advantages of two-photon microscopy, we employed this technique to further verify the probe's efficiency in detecting Hg²⁺ at the tissue and cellular level. To evaluate the probe's specificity in vivo (Fig. 3A and B), the model plant Arabidopsis thaliana was treated with various metal ions including Cd²⁺, Mg²⁺, Zn²⁺, K⁺ and Hg²⁺ respectively and then imaged under two-photon microscopy $(\lambda_{\rm ex} = 750 \text{ nm});^{34} \text{ only the Hg}^{2+} \text{ treated group showed}$ significant fluorescence signal output, indicating LJTP3 can be employed for Hg²⁺ specific imaging in plant tissues. As evidenced in Fig. S23,† two-photon comparative experiments were systematically conducted to examine the system before and after S²⁻ introduction. The experimental data demonstrate near-complete fluorescence quenching upon S²⁻ addition, strongly suggesting the reversible binding behavior between LJTP3 and Hg²⁺ in plant systems. In addition, the translocation of Hg²⁺ in plant tissues at the subcellular level, as well as the stress response of plant cells under Hg²⁺ exposure, were visualized in a real time manner (Fig. 3D and E). In the control group, where Hg^{2+} was absent, only a faint fluorescence signal was detected. However, after 1 hour of incubation with Hg²⁺, fluorescence corresponding to the probe's interaction with Hg²⁺ appeared on the epidermal cells of the root tip. After 3 hours, the fluorescence became more widespread, reflecting a significant uptake of the probe within the root tip cells. Moreover, after 5 hours, the fluorescence intensity increased markedly, indicating a strong and clear signal. Similar trends were observed in the Arabidopsis leaf epidermis (Fig. S21C and D ESI†).

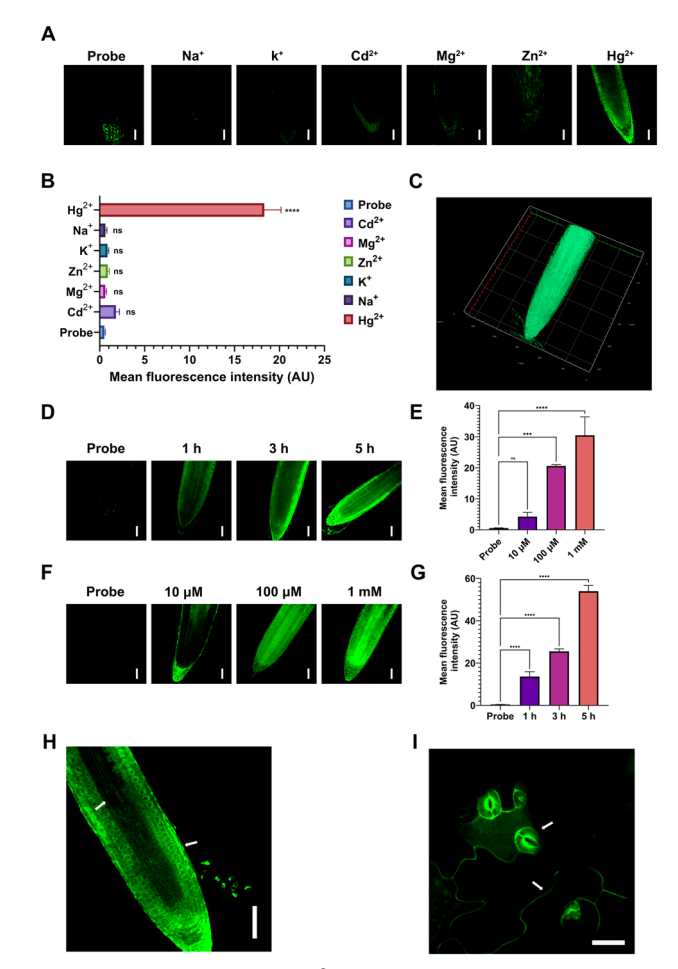


Fig. 3 In vivo imaging of Hg²⁺ with LJPT3. (A and B) Elemental selective imaging fluorescence pictures of LJPT3 and their quantitative data. (C) 3D reconstruction of LJPT3 signal distribution in plant roots. (D and E) Fluorescence pictures of Arabidopsis root tips under different Hg²⁺ treatment times and their quantitative data. (F and G) Fluorescence pictures of Arabidopsis root tips treated with different concentrations of Hg²⁺ and their quantitative data. (H) Fine structure imaging fluorescence picture of Arabidopsis root tips. (I) Fine structure imaging fluorescence picture of Arabidopsis leaf epidermis (scale bar = 50 μm).

To further investigate the fluorescence signal transmission in Arabidopsis under different Hg2+ concentrations, twophoton imaging was performed on root tips under varying Hg²⁺ stress levels (Fig. 3F and G). Only weak fluorescence signals were detected in the control group (no Hg²⁺ treatment). Under the stress of 10 µM Hg2+, fluorescence signals began to appear around the cells of Arabidopsis root tips. At 100 μM Hg²⁺, signals are present in most cells of the root tip. When the concentration was increased to 1 mM, signals appeared in all cells of the root tip and exhibited very high fluorescence intensity. In the leaf epidermis under the same treatment, the signal changed in a similar trend (Fig. S21A and B ESI†). The above results manifested that the dynamic distribution of Hg²⁺ can be visualized using LJTP3.

Under a single photon microscope with 3D imaging and reconstruction, LJPT3 can also directly visualize the spatial

distribution of Hg²⁺ in plant organs (Fig. 3C). In summary, LJPT3 can realize the non-destructive detection of Hg²⁺ in plant organs and tissues in a very short time, with good selectivity and sensitivity, and can accurately indicate the location and content of Hg²⁺ in plants.

To evaluate the capability of LIPT3 in detecting Hg²⁺ distribution differences within plant tissue microstructures, fluorescence signals in Arabidopsis root tips and leaf epidermis were analyzed using two-photon microscopy. Under 10 μM Hg²⁺ treatment, the root epidermis exhibited stronger fluorescence than the stele, reflecting a defense strategy against mercury. Likewise, the leaf epidermis showed higher fluorescence than the root stele, indicating differential Hg²⁺ accumulation (Fig. 3H), consistent with previous reports.

This disparity is attributed to plant cell defense mechanisms against Hg²⁺, aligning with previous findings.³⁵ In leaves, stomata exhibited stronger fluorescence than epidermal cells (Fig. 3I), as they serve as key sites for Hg²⁺ exchange between plants and the environment. Plants absorb elemental mercury via the stomata and convert accumulated mercury in leaves into elemental form for release.³⁶

In conclusion, we have designed a highly efficient fluorescent probe (LJTP3) specifically to study Hg²⁺ stress in plant tissues. LJTP3 demonstrated excellent selectivity and sensitivity for the early detection of Hg²⁺ in aqueous solution, with a detection limit of 0.08 µM. Remarkably, LJTP3 exhibited outstanding selectivity for Hg2+ in both in vitro tests and plant imaging. Moreover, under two-photon imaging, the distribution of Hg²⁺, along with Hg²⁺-induced rupture of root tip cells and leaf stomata, was clearly observed. We believe that this study not only provides a novel imaging tool for investigating Hg²⁺-induced stress on plant cell structures but also contributes to the management of Hg pollution in agriculture.

Data availability

The authors confirm that the data supporting the findings of this study are available within the article and its ESI.†

Author contributions

Shengzhen Xu and Jun Li conceived the basic idea and reviewed the manuscript. Xiao Liu designed and performed the experiment and drafted the manuscript. Zheng Zhu performed the experiments and imaging; Ruitao Sun provided suggestions on experiment. All authors read and approved the manuscript. Xiao Liu and Zheng Zhu contributed equally to this work.

Conflicts of interest

There are no conflicts to declare.

Acknowledgements

This work was financially supported by the Minhui Cao Studio of Huazhong Agricultural University.

Notes and references

- 1 C. T. Driscoll, R. P. Mason, H. M. Chan, D. J. Jacob and N. Pirrone, Environ. Sci. Technol., 2013, 47, 4967-4983.
- 2 Y. S. Wu, A. I. Osman, M. Hosny, A. M. Elgarahy, A. S. Eltaweil, D. W. Rooney, Z. H. Chen, N. S. Rahim, M. Sekar, S. C. B. Gopinath, N. N. I. M. Rani, K. Batumalaie and P. S. Yap, ACS Omega, 2024, 9, 5100-5126.
- 3 P. A. Nogara, C. S. Oliveira, G. L. Schmitz, P. C. Piquini, M. Farina, M. Aschner and B. T. Rocha, Biochim. Biophys. Acta, Gen. Subj., 2019, 1863, 129-284.
- 4 B. Gworek, W. Dmuchowski and A. H. Baczewska-Dąbrowsk, Environ. Sci. Eur., 2020, 32, 128.
- 5 J. Zhou, D. Obrist, A. Dastoor, M. Jiskra and A. Ryjkov, Nat. Rev. Earth Environ., 2021, 2, 269284.
- 6 W. Yuan, X. Wang, C. J. Lin, F. Wu, K. Luo, H. Zhang, Z. Y. Lu and X. B. Feng, Environ. Sci. Technol., 2022, 56, 14154-14165.
- 7 S. Li, C. C. Zhang, S. N. Wang, Q. Liu, H. H. Feng, X. Ma and J. H. Guo, Analyst, 2018, 143, 4230-4246.
- 8 T. A. Saleh, G. Fadillah, E. Ciptawati and M. Khaled, TrAC, Trends Anal. Chem., 2020, 132, 116016.
- 9 K. Schlöglova, M. Wälle and C. A. Heinrich, J. Anal. At. Spectrom., 2017, 32, 1052-1063.
- 10 K. Srinivasan, K. Subramanian, A. Rajasekar, K. Murugan, G. Benelli and K. Dinakaran, Bull. Mater. Sci., 2017, 40, 1455-1462.
- 11 M. C. Dai, Y. J. Yang, S. Sarkar and K. H. Ahn, Chem. Soc. Rev., 2023, 52, 6344-6358.
- 12 X. L. Ding, Q. Wang, D. Chen, Y. L. Chen, W. W. Pan, Q. Sun, Q. Chen and X. Y. Han, Adv. Agrochem, 2023, 2, 364-370.
- 13 J. Yin, Y. Hu and J. Y. Yoon, Chem. Soc. Rev., 2015, 44, 4619-4644.
- 14 Z. J. Zhang, B. R. Adhikari, P. Sen, L. Soleymani and Y. F. Li, Adv. Agrochem, 2023, 2, 246-257.
- 15 J. Li, D. Yim, W.-D. Jang and J. Yoon, Chem. Soc. Rev., 2017, 46, 2437-2458.
- 16 L. H. Feng, Y. Deng, X. J. Wang and M. G. Liu, Sens. Actuators, B, 2017, 245, 441-447.
- 17 G. J. Li, J. L. Wang, D. Y. Li, S. H. Liu, J. Yin, Z. B. Lai and G. F. Yang, Chin. Chem. Lett., 2021, 32, 1527-1531.
- 18 J. H. Wang, Y. M. Liu, Z. M. Dong, J. B. Chao, H. Wang, Y. Wang and S. M. Shuang, J. Hazard. Mater., 2020, 382, 121056.
- 19 L. N. Neupane, J. Park, P. K. Mehta, E. T. Oh, H. J. Park and K. H. Lee, Chem. Commun., 2020, 56, 2941-2944.
- 20 Z. G. Wang, Y. Zhang, J. Yin, Y. Q. Yang, H. Luo, J. Song, X. Xu and S. F. Wang, ACS Sustainable Chem. Eng., 2020, 33, 12348-12359.
- 21 L. Wang, Y. Ma and W. Y. Lin, J. Hazard. Mater., 2024, 461,

- 22 Y. Y. Zhang, W. Shi, D. Feng, H. M. Ma, Y. Liang and J. R. Zuo, Sens. Actuators, B, 2011, 153, 261-265.
- 23 Y. Yang, R. Shen, Y. Z. Wang, F. Z. Qiu, Y. Feng, X. L. Tang, D. C. Bai, G. L. Zhang and W. S. Liu, Sens. Actuators, B, 2018, 255, 3479-3487.
- 24 K. Ramki, G. Thiruppathi, S. K. Ramasamy, P. Sundararaj and P. Sakthivel, Methods, 2024, 221, 1-11.
- 25 H. Y. Niu, T. Q. Ye, L. Y. Yao, Y. F. Lin, K. Chen, Y. B. Zeng, L. Li, L. H. Guo and J. B. Wang, J. Hazard. Mater., 2024, 475, 134914.
- 26 Y. An, B. Li, Y. Z. Yu, Y. C. Zhou, J. F. Yi, L. P. Li, Y. Q. Sun, Z. Z. Qiang, Y. Q. Liu and P. Wang, J. Hazard. Mater., 2024, 465, 133331.
- 27 C. Zhao, A. Aziz, W. J. Lu, H. M. Xu, M. Asif, S. M. Shuang and C. Dong, J. Hazard. Mater., 2024, 479, 135694.
- 28 J. H. Wang, Y. M. Liu, Z. M. Dong, J. B. Chao, H. Wang, Y. Wang and S. M. Shuang, J. Hazard. Mater., 2020, 382, 121056.

- 29 J. Z. Du, K. M. Chen, Z. Y. Yu, Y. H. Qiao, J. X. Liu, Q. Q. Zhai, Z. Hu, S. G. Yang, J. Li and H. L. Teng, Adv. Agrochem, 2022, 1, 162-173.
- 30 V. Juvekar, S. J. Park, J. Y. Yoon and H. M. Kim, Coord. Chem. Rev., 2021, 427, 213574.
- 31 H. W. Lee, V. Juvekar, D. J. Lee and H. M. Kim, TrAC, Trends Anal. Chem., 2023, 165, 117128.
- 32 S. Asghar, Z. Yu, Z. Zhu, D. Zheng, Z. Zhao, Y. Xu, X. Liu, C. Yuan, Y. Li, W. Wang, J. F. Xu, H. L. Teng, J. Li, W. C. Yang and C. Chen, Research, 2025, 8, 0570.
- 33 G. J. Li, J. L. Wang, D. Y. Li, S. H. Liu, J. Yin, Z. B. Lai and G. F. Yan, Chin. Chem. Lett., 2021, 32, 1527-1531.
- 34 H. J. Kim, J. H. Han, M. K. Kim, C. S. Lim, H. M. Kim and B. R. Cho, Angew. Chem., 2010, 122, 6938-6941.
- 35 J. J. Wang, Y. Y. Guo, D. L. Guo, S. L. Yin, D. L. Kong, Y. S. Liu and H. Zeng, Environ. Sci. Technol., 2012, 46, 769-777.
- 36 W. Yuan, X. Wang, C. J. Lin, F. Wu, K. Luo, H. Zhang, Z. Y. Lu and X. B. Feng, Environ. Sci. Technol., 2022, 56, 14154-14165.